BULLETIN OF THE POLISH ACADEMY OF SCIENCES
TECHNICAL SCIENCES
Vol. 53, No. 2, 2005

High power QW SCH InGaAs/GaAs lasers for 980-nm band

M. BUGAJSKI*, B. MROZIEWICZ, K. REGIŃSKI, J. MUSZALSKI, K. KOSIEL, M. ZBROSZCZYK, T. OCHALSKI, T. PIWOŃSKI, D. WAWER, A. SZERLING, E. KOWALCZYK, H. WRZESIŃSKA, and M. GÓRSKA

Institute of Electron Technology 32/46 Lotników Ave., 02 668 Warszawa, Poland

Abstract. Strained layer InGaAs/GaAs SCH SQW (Separate Confinement Heterostructure Single Quantum Well) lasers were grown by Molecular Beam Epitaxy (MBE). Highly reliable CW (continuous wave) 980-nm, broad contact, pump lasers were fabricated in stripe geometry using Schottky isolation and ridge waveguide construction. Threshold current densities of the order of $J_{th} \approx 280$ A/cm^2 (for the resonator length L = 700 μm) and differential efficiency $\eta = 0.40$ W/A (41%) from one mirror were obtained. The record wall-plug efficiency for AR/HR coated devices was equal to 54%. Theoretical estimations of above parameters, obtained by numerical modelling of devices were $J_{th} = 210$ A/cm and $\eta = 0.47$ W/A from one mirror, respectively. Degradation studies revealed that uncoated and AR/HR coated devices did not show any appreciable degradation after 1500 hrs of CW operation at 35°C heat sink temperature at the constant optical power (50 mW) conditions.

Key words: laser diodes, strained-layer semiconductor lasers.

1. Introduction

Quantum well separate confinement heterostructure lasers (QW SCH) are usually designed with single quantum well (SQW) or multiple quantum well (MQW) active region. Multiple quantum well active region leads to effective increase of the electrically pumped volume and thus allows for obtaining high powers which are attractive for such applications as diode pumped Nd:YAG lasers. The price one pays for higher power, however is an increased threshold current density, since for reaching a necessary inversion level one has to fill with carriers a few quantum wells [1,2]. Available experimental data show that also the other parameters of the laser depend on whether the active region is single or multiple quantum well [3,4]. Theoretical works published so far reflected in general observed experimental trends [5–9]. Nonetheless, since they have used threshold analysis of the laser, based on the balance of gain and losses and employed a number of phenomenological parameters, in particular semi-empirical gain model and simplified band structure, they were not been able to predict more sophisticated effects. It has to be also stressed that models in question were originally developed for double heterostructure (DH) lasers [10] and were subsequently used, with only minor modifications, for quantum well lasers where they do not fully reflect physical complexity of involved phenomena. The reason for that was their simplicity and low computational requirements. Assuming the technological importance of semiconductor lasers, it is crucial to be able to perform predictive modelling of new device designs before actual manufacturing devices. In this work an attempt has been made to use more rigorous approach to laser modelling, based on self-consistent solution of transport equations and Schroedinger equation. The calculations have been applied to strained layer 980-nm InGaAs/GaAs SCH QW lasers.

The development of erbium-doped fiber amplifiers (EDFA) has enabled the proliferation of high-bandwidth data networks. Er^{3+}-doped fiber amplifiers coherently amplifying 1550-nm signals through the conversion of 980-nm pump laser light [11]. Because the process is all optical, many signals can be amplified simultaneously with no delay and minimal electronics is required. The use of 980-nm pump wavelength has also another advantage as no excited state absorption exists for this wavelength. The pump lasers powering EDFAs must be highly reliable and at the same time have to provide maximum amplification power. All practical 980-nm lasers are based on the ternary AlGaAs and InGaAs alloys. The excellent lattice match, refractive index contrast, and thermal conductivity of AlGaAs give a freedom to optimize the vertical laser structure, while a single pseudomorphic InGaAs quantum well active region produces enough gain and good electrical confinement leading to low-threshold current and high quantum efficiency [12,13]. Technology of growth of SCH SQW structures has been developed to practical measures due to ours previous experiences with AlGaAs/GaAs semiconductor lasers fabricated at the Institute of Electron Technology [14,15].

2. Laser design and threshold analysis

The laser structures were designed for 980-nm operation at room temperature (T = 300 K). The required wavelength can be obtained by adjusting In content in the

*e-mail: bugajski@ite.waw.pl

active layer and the thickness of the quantum well. Assuming $\sim 20\%$ In content in InGaAs QW, the thickness of the quantum well has been estimated roughly to be in the range between 60 Å and 100 Å to give the emission in the 980-nm range. This has been generally verified by PL measurements on the grown test structures. The laser simulation has been performed using commercial PICS 3D software package [16]. Typically, besides emission spectra, P-I (optical power-current) characteristics for lasers with stripe contact and different resonator lengths are calculated. The calculated threshold current densities have to be understood as a bottom limit; in actual devices one should expect the higher values, due to unavoidable technological and processing faults and inaccuracies. Numerical simulation gives us guidelines for designing lasers and optimizing their performance and speeds up development of practical devices. Since laser performance optimization has to be subjected to numerous restrictions (material and technological), the numerical modelling is an indispensable tool saving many efforts which would be otherwise spent on technological experiments.

2.1. Physical basis of laser symulator. Basic equations describing operation of semiconductor laser are Poisson's equations:

$$-\nabla\left(\frac{\varepsilon\varepsilon_0}{e}\nabla V\right) = -n + p + N_D\left(1 - f_D\right) - N_A f_A + \sum_j N_{tj}\left(\delta_j - f_{tj}\right) \quad (1)$$

and continuity equations for electrons and holes

$$\nabla J_n - \sum_j R_n^{tj} - R_{sp} - R_{st} - R_{au} = \frac{\partial n}{\partial t} + N_D\frac{\partial f_D}{\partial t} \quad (2)$$

$$\nabla J_p + \sum_j R_p^{tj} + R_{sp} + R_{st} + R_{au} = -\frac{\partial n}{\partial t} + N_A\frac{\partial f_A}{\partial t} \quad (3)$$

The above equations govern electrical characteristics of the device (e.g., I–V characteristics). Analysis of the optical characteristics requires the solution of Helmholtz equation, describing optical field distribution in the resonator.

$$\nabla^2 W + k_0^2\left(\varepsilon - \beta^2\right)W = 0 \quad (4)$$

The densities of electron and hole currents Jn and Jp can be expressed as a function of free carrier concentrations and variations of respective quasi-Fermi levels.

$$J_n = n\mu_n\nabla E_{fn} \quad (5)$$

$$J_p = p\mu_p\nabla E_{fp} \quad (6)$$

Laser simulator solves self-consistently the above set of partial differential equations for electrostatic potential V, electron and hole concentration n and p, optical field distribution W and photons number in the resonator S. For the analysis of semiconductor laser it is important to evaluate the carrier density and the optical gain of a quantum well. The standard approach to the modelling is based on the parabolic band model. It is the most efficient model and usually it reproduces the general trends with satisfactory accuracy. For more accurate calculations, especially in the case of strained layer InGaAs/GaAs lasers one has to relay on more elaborate models. Inclusion of the biaxial strain in the design of quantum well semiconductor lasers provides an additional degree of freedom and produces some desirable effects, such as lower threshold current. The effects of strain are described theoretically using $\boldsymbol{k}\,\boldsymbol{p}$ description of the band structure in the quantum well. This type of calculation up to now has limited capability in analyzing practical design issues and optimization of laser geometry. The approximate treatment of the strain is based on the approximation of non-parabolic band structure by an anisotropic parabolic one (with proper inclusion of strain-induced shifts and splitting of light hole (LH) and heavy hole (HH) bands). The calculations are based on analytical approximation to the band structure of strained quantum well, which has been developed recently [17] using an efficient decoupling method to transfer the 4×4 valence band Hamiltonian into two blocks of 2×2 upper and lower Hamiltonians. As a result of the decoupling, analytical expressions for in plane valence sub-bands dispersion relations can be derived. Once the parabolic subbands are found, one can apply conventional approaches to treat carrier concentration and the optical transition probabilities. The effective mass perpendicular to the quantum well plane determines the quantum sub-band energies at $\boldsymbol{k} = 0$, while the densities of states for each sub-band are determined using the in plane effective masses. In the framework of the model developed in [17] it is also possible to account for anticrossing behaviour of the valence band sub-bands (i.e., valence band mixing).

With no carrier injection the active layer material is strongly absorbing. With carrier injection we can invert the carrier population near the band edge and convert absorption into gain. The region of positive gain exists in limited energy range above the bandgap of the material. It extends between the bandgap and the quasi-Fermi level separation: $E_g < h\nu < \triangle E_g$ The spectral shape of the QW gain and peak gain on injected carrier density expressions differ considerably from that of bulk material. These differences are the consequences of the step-like density of states in QW material. Apart from this, the derivation of appropriate expression for gain follows usual treatment. The optical gain is calculated using standard perturbation theory (Fermi's Golden Rule). The spectrally dependent gain coefficient can be written in the form,

$$g(E) = \frac{q^2|M|^2}{E\varepsilon_0 m^2 c\hbar N L_z}\times \sum_{i,j} m_{r,ij}C_{ij}A_{ij}\left[f_c - (1 - fv)\right]H\left(E - E_{ij}\right) \quad (7)$$

where: $|M|^2$ – bulk momentum transition matrix element; C_{ij} – spatial overlap factor between states i and j; A_{ij} – anisotropy (polarization) factor for transition i, j; $m_{r,ij}$ – spatially weighted reduced mass for transition i, j; E_{ij}

– transition energy between states i and j; N – effective refractive index; H – Heaviside step function; i, j – conduction, valence (lh, hh) quantum numbers at Γ point. For the perfectly confined QW states $\Delta n = 0$ selection rule applies. The reduced mass parameter is given by $m_{r,ij}^{-1} = m_i^{-1} + m_j^{-1}$, where m_i and m_j are weighted (by wave function confinement factor in QW) averages of QW and cladding masses.

Momentum conservation restricts the energies of the initial and final states. The bulk averaged momentum matrix element between the conduction and valence states is:

$$|M|^2 = \frac{m^2 E_g \left(E_g + \triangle\right)}{6m_c \left(E_g + 2\triangle/3\right)} \tag{8}$$

The angular anisotropy factor is normalized so that its angular average (bulk limit) is unity. For the TE transitions, with the electric field vector in the plane of the QW, its values are: $A_{ij} = 3/4\left(1 + \cos^2\theta_{ij}\right)$ for *e-hh* transitions and $A_{ij} = 1/4\left(5 - 3\cos^2\theta_{ij}\right)$ for *e-lh* transitions. The bands are assumed to be parabolic in first approximation, thus the occupation density of the *i-th* (conduction or valence) band is:

$$n_i, p_i = \frac{kTm_i^{c,\nu}}{\pi\hbar^2 L_z} \ln\left[1 + \exp\left(\frac{E_f^{c,\nu} - E_i^{c,\nu}}{kT}\right)\right] \tag{9}$$

where the quasi-Fermi energies E_f and the quantum levels E_i are measured positive into respective band from the $k = 0$ band edge. We assume undoped QW with high injection, so the charge neutrality gives the condition $n = p_{lh} + p_{hh}$. The carrier scattering processes are accounted for by introducing appropriate broadening of the quantum levels. The net effect of this broadening can be found by convoluting the Lorentzian shape function with gain distribution ($g'(E) = g(E) \times L(E)$). The broadening significantly reduces the local gain. The discussed relations allow for calculating gain vs. injected carrier density.

The above equations give the material gain of quantum well in terms of carrier density, which is not directly measurable. From the point of view of calculating properties of semiconductor injection laser the relation between the current and carrier density must be established by balancing current with total carrier recombination rate which consists of radiative and non-radiative components. The radiative component of carrier recombination is found from spectrally dependent spontaneous emission rate. The non-radiative contribution to the current comes mainly from thermal leakage current and from Auger recombination. The most common method of estimating Auger recombination is to use experimentally obtained Auger coefficients in combination with calculated carrier density ($R_A = CN^3$). Theories can predict Auger rate to within an order of magnitude. In quantum-well lasers carriers can leak into separate confinement waveguiding layers as well as leaking out of the entire SCH waveguide region into the doped cladding layers has to be considered. Carrier population in the SCH region leads to recombination giving leakage current density of the order of 50 A/cm^2 per 10^{17} cm^{-3} of carrier density. This shows the importance of maintaining low carrier density in the waveguide regions of the laser.

The theory of gain based on Fermi's Golden Rule considers each electron in isolation as it interacts with electromagnetic field, i.e., it is a single-particle theory and as such it neglects mutual interactions between electrons. The physical consequences of many-body effects in dense electron plasma in QWs are basically of two types: excitonic effects and bandgap renormalization effects. The first one will result essentially in the changes of the spectral shape of material gain curves and will be enhanced in quantum wells comparing to the bulk material. The second will produce the bandgap shrinkage due to the combined exchange and correlation effects. The net effect of the bangap shrinkage is the noticeable red-shift of gain spectrum accompanied by its reshaping and enhancement. This phenomenon is clearly observable in quantum well lasers where the high threshold carrier density shifts the lasing wavelength beyond the known band edge wavelength of the quantum well. Nevertheless, all practical laser simulators available now are based on free-carrier gain model, which is easier to implement numerically. The full account of many-body laser theory can be found in the monograph [18].

2.2. Numerical simulation of SCH SQW InGaAs/GaAs laser. The sketch of the typical device simulated is shown in Fig.1. The sequence of layers consists of n-type GaAs buffer, the $Al_xGa_{1-x}As$ n-type barrier layer, undoped active layer and waveguide, the $Al_xGa_{1-x}As$ p-type barrier layer and p$^+$-type GaAs sub-contact layer. Active layer is composed of $In_yGa_{1-y}As$ quantum well enclosed by GaAs waveguide. The model was tested for different values of structure parameters, i.e., thickness of individual layers, composition and doping. The indium content in InGaAs QW was varied from $y = 0.20$ to $y = 0.22$ and the well thickness from 60 Å to 100 Å. The AlGaAs compositions $x = 0.30$ and $x = 0.70$ were tested. Finally we have studied the influence of the thickness of GaAs waveguide, which had been changed from 0.1 μm on each side of QW to 0.3 μm, on the laser characteristics. The doping of both emitters was kept on 5×10^{17} cm^{-3} level for all simulations. Such complex

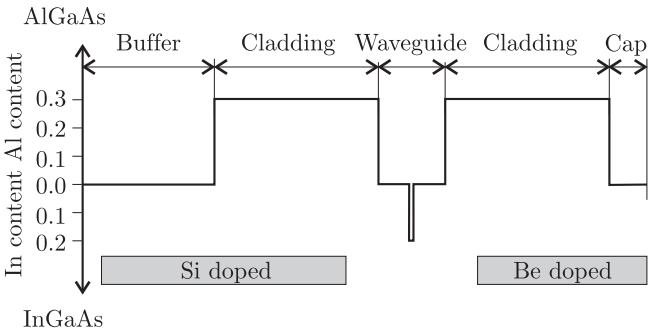

Fig. 1. SCH SQW InGaAs/GaAs strained layer laser structure

program of investigations would be difficult to realize by relaying exclusively on technological experiments. Nevertheless, the key numerical results were confronted with real experiments to verify calculations and provide solid foundations for hypothesis derived from numerical experiments. Such combined approach proved to be very successful in developing 980-nm lasers.

Typical, calculated P-I (optical power-current) characteristics for lasers with stripe width $W = 100$ μm and resonator length $L = 700$ μm are shown in Fig. 2. Threshold current densities for modelled lasers are equal to 197 A/cm^2 and 208 A/cm^2, depending on construction details, which are in agreement with values obtained experimentally by Coleman [12] for broad area strained-layer InGaAs/GaAs lasers of similar geometry but with higher Al content in the emitters. The majority of early lasers were GRIN SQW type, while now simple SCH SQW or SCH MQW lasers, as studied in this work, dominate, which in most cases makes comparison of calculated results with available experimental data only approximate – but general trends are reproduced properly. The calculated threshold current densities have to be understood as a bottom limit; in actual devices one should expect the higher values, due to unavoidable technological and processing faults and inaccuracies.

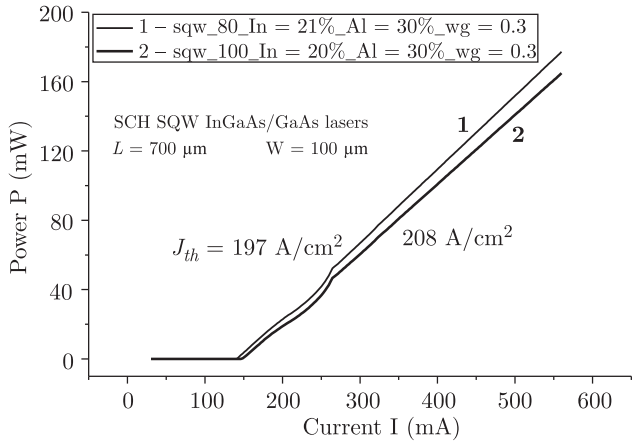

Fig. 2. Calculated P-I characteristics of SCH SQW InGaAs/GaAs lasers

Application of narrower waveguiding layer (∼ 0.1 μm on each side of the quantum well) decreases threshold current by about 25% (cf. Fig. 3) but on the other hand optical power density in the resonator increases roughly 3 times. This may lead to a faster degradation of lasers, in particular to the lowering of COD (Catastrophic Optical Damage) threshold level. The heat generated by the absorption of laser radiation at the mirrors can result in irreversible damage of the laser. Since our primary concern was durability of lasers the former design, with broader waveguide, was chosen although the penalty of slightly higher threshold had to be paid. Extremely low threshold current densities, of the order of 120 A/cm^2, can be obtained using both narrow waveguide (∼ 0.1 μm) and high Al content ($x = 0.70$) in the emitters. Such construction can be useful for low power, high-speed lasers with narrow stripes (5 μm–10 μm) operated at low drive currents.

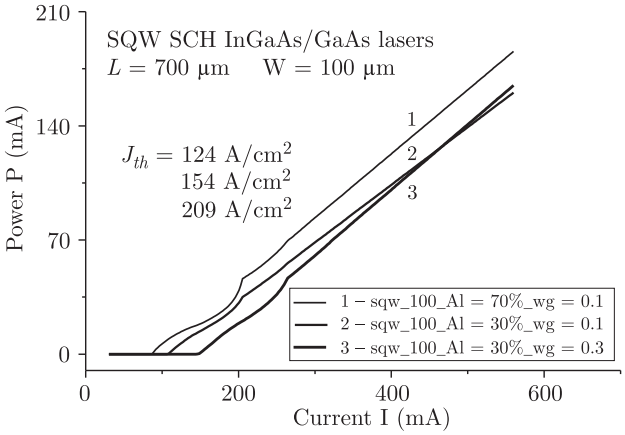

Fig. 3. Calculated P-I characteristics of SCH SQW InGaAs/GaAs lasers with different waveguide thickness

The influence of QW thickness, with the other construction details unchanged, on laser parameters has been also studied. The results of calculation show that differential quantum efficiency of the laser (η) grows with decreasing QW thickness, reaching 0.54 W/A (42.7%) for $L = 60$ Å. On the other hand, the threshold current density J^{th} reaches minimum 121 A/cm^2 for $L = 80$ Å. The results suggest that a good optimization procedure would be to choose QW thickness $L = 80$ Å and vary In content in the active region to get required wavelength of laser emission, i.e., 980 nm. The thickness of both emitters should be at least 1.0 μm each, preferably 1.5 μm, to assure that optical field of the fundamental mode does not penetrates the highly absorbing GaAs regions.

The final laser structure has been decided according to the simulation results. The thickness, composition and doping of individual layers constituting the structure were chosen as listed in the Table 1.

Tabele 1
Typical parameters of SCH SQW InGaAs/GaAs/AlGaAs laser structures

Buffor	n-emiter	Waveguide	QW	Waveguide	p-emiter	Cap
1 μm GaAs:Si	1 μm – 1.5 μm	0.1–0.3 μm	80 Å	0.1–0.3 μm	1 μm – 1.5 μm	0.25 μm
$n = 2\times10^{18}$cm^{-3}	$Al_xGa_{1-x}As$:Si	GaAs	$In_xGa_{1-x}As$	GaAs	$Al_xGa_{1-x}As$:Be	GaAs:Be
0.2 μm	$x = 0.3$		$x = 0.20$–0.22		$x = 0.3$	
$Al_xGa_{1-x}As$:Si	$n = 5\times10^{17}$cm^{-3}	undoped	undoped	undoped	$p = 5\times10^{17}$cm^{-3}	$p = 3\times10^{19}$cm^{-3}
$x = 0.0$-0.3						
$n = 5\times10^{17}$cm^{-3}						

SCH SQW laser structures were grown by molecular beam epitaxy (MBE) in Riber 32P reactor in a manner similar to previously described [19].

The structures were grown on (100) GaAs conductive substrates. The sequence of layers for typical, optimized for reliable high power CW operation, structure consisted of n-type GaAs buffer, the $Al_{0.3}Ga_{0.7}As$ n-type barrier layer, undoped active layer and waveguide, the $Al_{0.3}Ga_{0.7}As$ p-type barrier layer and p^+-type GaAs subcontact layer. Active layer and waveguide comprised of $In_{0.21}Ga_{0.79}As$ 80 Å quantum well enclosed by 0.3 μm GaAs layers.

3. Strained-layer laser structures – MBE growth related issues

The growth of InGaAs/GaAs heterostructures is much more difficult than the growth of AlGaAs/GaAs ones. The reason for that is large lattice mismatch between substrate and the growing layer. The lattice constant of GaAs is equal to 5.6533 Å, whereas that of InAs equals 6.0584 Å, which results in 7% lattice mismatch between those two semiconductors and precludes the growth of high indium containing InGaAs on GaAs substrate. The room temperature band gap of $In_xGa_{1-x}As$ ternary alloy varies from 1.424 eV (GaAs) to 0.36 eV (InAs). The energy range close to 1.424 eV is attainable by using $In_xGa_{1-x}As$ layers grown on GaAs substrates. This way the layers with indium content up to 0.2 and reasonable thickness up to 100 Å can be grown [20]. The layer with different lattice constant than that of the substrate undergoes a tetragonal deformation during the growth. Depending on whether the lattice constant of the layer is greater or smaller than the lattice constant of the substrate, we have biaxial compressive or biaxial tensile strain in the plane of the layer and appropriate deformation of the elementary lattice cell in perpendicular direction for which the strain is relaxed. With increase of the layer thickness, the elastic deformation energy stored in the crystal grows and when its value exceeds certain threshold value determined by the Hook's law the stress is released and the misfit dislocations are formed [21]. The thickness of the layer for which stress relaxation occurs is called a critical thickness. It depends mainly on the lattice mismatch between the layer and the substrate. For the materials with large lattice mismatch, such as InGaAs on GaAs, the critical thickness values are few orders of magnitude smaller than that for AlGaAs on GaAs with a similar composition. The lattice mismatch is the main factor responsible for difficulties encountered in the growth of InGaAs on GaAs. The growth of lattice mismatched layers can be realized only in the limited range of thickness and compositions and even then is a difficult task, requiring a precise knowledge of the phenomena occurring in strained materials.

Band structure of III–V semiconductor compounds changes appreciably under biaxial strain originating in thin layers of these materials grown on lattice mismatched substrates. The presence of strain removes degeneracy of valence band $k = 0$, changes band gap as well as dispersion relation in the valence band. In quantum wells the influence of strain is even more complicated. All these changes can be positively exploited in designing quantum well lasers, resulting in improved device characteristics and flexibility in fabricated lasers parameters [22]. Penalty paid for this is difficult growth technology. Quality of interfaces and defects in strained layer semiconductor structures greatly affect parameters of lasers. Roughness of surfaces is cause of dissipative loss of emission and probable non-radiative recombination on defects involved. Because of that total internal losses increase which leads to higher threshold current and decrease of quantum efficiency of the lasers. This finally causes decrease of external differential efficiency (slope of optical power vs. current characteristics is smaller). To achieve as smooth as possible and defect free interfaces (in particular the most important are interfaces between quantum well and waveguide) we have applied photoluminescence measurements performed on as grown structures [23].

The performance and reliability of semiconductor lasers depends critically on the crystal growth technique. In this respect, lasers are probably the most demanding III–V minority carrier devices. Fabrication of high quality laser structures by MBE needs a careful optimization of the growth conditions. From the point of view of MBE technology several factors are of great importance: high purity and structure perfection of undoped layers, the relevant profiles of dopant concentration, good quality of interfaces, high dopant concentration in contact layers, etc. Therefore, the optimization of the MBE process comprises the determination of the growth conditions for each layer of the laser structure. The growth must proceed with right combination of temperatures of substrate and ratios of group V/III atomic beams, which guarantee appropriate reconstruction of surface and proper growth conditions for each layer, which indeed vary appreciably. This allows us to achieve layers of the best optical quality.

In general AlGaAs should be grown at as high temperatures as possible and at low V/III ratio (to minimize oxygen content in the layers), whereas InGaAs prefers substantially lower temperatures and higher V/III beam ratios. Fulfilling these conditions requires abrupt changes of beam fluxes which is difficult to realize due to thermal inertia of effusion cells. To avoid process interruptions at the surfaces we have used two arsenic cells preheated at different temperatures. To monitor the state of the crystal surface at any stage of the growth process the RHEED (Reflection High Energy Electron Diffraction) system was used. The RHEED patterns were registered by CCD camera and then processed in real time and recorded by a computer acquisition system. The system enabled us to register RHEED intensity oscillations and, as a result, to determine the growth rate. As a result, we had at our disposal two independent methods of measuring the growth rate. The first one based on the measurement of atomic

Table 2
Optimized MBE growth conditions for InGaAs/GaAs laser structures

Material	Layer	T (°C)	Growth rate (μm/hr)	V/III flux ratio	Reconstruction
GaAs	buffer	580	0.8	4–5	(2×4)
	waveguide	550–580			
	subcontact	540			(3×1)
$Al_{0.30}Ga_{0.70}As$	emitters	690	1.15	2.1	(3×1)
$In_{0.20}Ga_{0.80}As$	QW	550	1.0	4	(2×4)

fluxes and the second one based on registering the RHEED intensity oscillations. That additional possibility strengthened our control over growth process and turned out to be crucial in developing the technology of laser structures. The analysis of RHEED diffraction patterns allowed us to determine substrate reconstruction for the case of growth of different materials composing laser structure, depending on the temperature and respective beam fluxes. It is well known that the quality of layers and their usefulness for certain applications can be linked to the type of surface reconstruction during the growth. For GaAs there are known types of reconstruction which produce layers especially suitable for optical applications. In the case of InGaAs the subject is less studied but the general trends are similar. Based on our previous experiences with GaAs/AlGaAs system and research done for this work we have found the set of optimum growth conditions (in terms of beam fluxes, surface reconstruction and temperatures) for the growth of InGaAs/GaAs/AlGaAs strained layer structures. They are listed in Table 2.

Optimized MBE growth parameters allowed for the growth of defect free laser structures in the whole range of indium content in the active region studied (0.10–0.25 mole fraction of In). Quality of the structures was routinely studied by PL (photoluminescence), PR (photoreflectance) and occasionally by TEM.

4. Device fabrication and laser characteristics

The broad contact (100 μm stripe width) ridge-waveguide lasers were fabricated from SCH SQW structures following a standard processing procedures used previously for DH AlGaAs/GaAs lasers. The AuGeNi/Au contact with additional thick Au layer was used for n-side of the device. The p-contact comprised of the following sequence of layers: Cr (50 nm), Pt (200 nm), Cr (50 nm) and Pt (150 nm). The individual lasers were In-soldered, p-side down, on copper blocks and contacted by a gold wire. The p-side down soldering of lasers has an advantage over n-side down mounting manifesting in better heat sinking, although it is much more difficult technologically and generally results in lower yield. The laser chip and the structure soldered to copper heat sink are shown in Fig. 4a and 4b, respectively. All laser chips were tested before soldering, using needle probe and micromanipulator. The P-I characteristics and spectral characteristics were measured. The CCD camera was used to observe near-field picture of laser emission. Light from the laser was delivered to the spectrometer using optical fiber. The measurements of laser characteristics, data acquisition and data processing were controlled by PC computer. For selected devices angular distribution of laser emission in two perpendicular directions (far-field pattern) was also recorded. Finally, devices were encapsulated in metal cases with window. Some of the lasers had antireflection (AR) and high-reflectivity (HR) coatings deposited on the front and rear facets respectively. One layer of SiO_2 was used for AR coating and Si/SiO_2 multilayer was used for HR-coating. The AR, HR coatings were deposited on lines of lasers, before dividing them into individual chips.

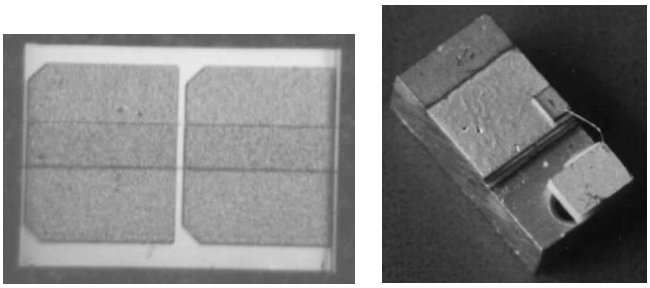

(a) (b)

Fig. 4. The laser chip (a) and the structure soldered to copper heat sink (b)

The preliminary results of works on 980-nm lasers have been published in series of recent papers of the authors [24–26]. Here we report updated results on degradation studies and selected best characteristics of the lasers. Fabricated lasers exhibited similar characteristics to the other structures of this type published in the literature [27–31]. Threshold current densities of the order of $J_{th} \approx 280$ A/cm^2 (for the resonator length $L = 700$ μm) and differential quantum efficiency $\eta = 0.40$ W/A (41%) were obtained. The wall-plug efficiency of the lasers without AR coating reached 38%. The optical power-current characteristics (P-I) for lasers fabricated from the same wafer showed almost equal thresholds and slightly different differential efficiencies. The linearity of the characteristics was good; there was no kinks and thermal roll-over for highest powers observed. The characteristics were typically recorded for pulse operation with filling factor $ff = 0.1\%$ (pulse length 200 ns, repetition 5 kHz).

Theoretical estimation of threshold current density and differential efficiency obtained by numerical modelling of the devices were $J_{th} \approx 210$ A/cm^2 and $\eta = 0.47$

W/A, respectively. The obtained experimentally threshold currents are fully acceptable, whereas differential efficiency could have been still improved. They lower than theoretically predicted value is most probably caused absorption losses in the cavity. Further work aimed on lowering absorption losses is required. The lasers generated at 980 nm – 990 nm wavelength range, depending on the part of the wafer from which they have been made, with the half-width of the emission band of the order of 1 nm, just above the threshold and up to 3 nm at high currents (high optical power). Emission spectrum contained many well-distinguished longitudinal modes, belonging to the fundamental transverse and lateral modes. As it has been mentioned earlier the requirement of precise wavelength control demanded by application of the devices as a pump source for Er^{3+}-doped amplifiers is difficult to fulfil but manageable. Besides the variation of the wavelength over the wafer, there are global variations between different MBE runs. Usually, the best reproducibility is achieved when one grows a series of 2" wafers with laser structures, without interruption for other processes. That assures a maximum stability of growth parameters.

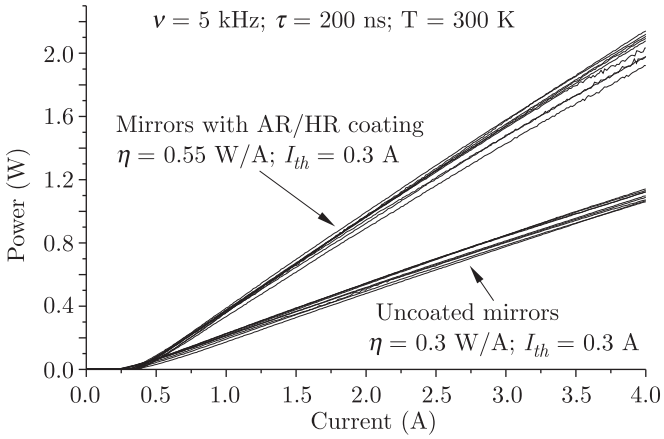

Fig. 5. Comparison of P-I characteristics of lasers with or without AR/HR coatings

To force laser emission through one, selected mirror one has to apply AR/HR coating. The other benefits of dielectric passivation of the mirrors is theoretically doubled differential efficiency of the laser and higher resistivity to degradation. The last particularly refers to increased COD level and greatly enhanced durability. According to recent reports [32], strained-layer InGaAs/GaAs lasers without mirror coating lived in CW regime on average about 250 hrs, whereas the lifetime of those with AR/HR coatings reached 5000–10000 hrs. Typical light-current characteristics of the lasers without AR/HR coatings and with AR/HR coatings, from one lot, are compared in Fig. 5. The threshold current of lasers with AR/HR coatings was unchanged comparing to uncoated ones but we have observed roughly twice increase in differential quantum efficiency. The record wall-plug efficiency for AR/HR coated devices was equal to 54%. Which is among the best values obtained for that type of lasers.

For some lasers we have performed aging tests. The lasers for the tests were selected on the basis of initial screening based on threshold current determination. Only the lasers with threshold within the limit of up to twice the average threshold have been subjected to lifetime testing. No special effort was made to select particularly good devices, rather we tried to chose a spectrum of different initial quality devices. Fabricated lasers showed in general good reliability. The uncoated devices, did not show an appreciable degradation after over 1000 hrs of CW operation at 35°C heat sink temperature, with 50 mW emitted power (in a constant power mode). This result can be extrapolated to 10^6 hrs of pulse operation with $ff = 0.1\%$. In the light of the results published in literature [32] this is extremely good result, even having in mind that the lasers with whom we compare our results were operated at 100 mW optical power. A total of 10 devices were placed on life test. The lasers with coated mirrors are at the moment of writing this paper still operated at the aging frame and their CW working time reaches 1500 hrs. Only one of them failed during the test and the rest maintan basicaly unchanged current. This is to be compared with typical CW operating times of a few khrs, published in the literature [33–35]. The apparent immunity of investigated lasers to sudden failure is striking and despite the small statistical base it is undoubtedly an inherent property of strained-layer InGaAs/GaAs lasers as compared to conventional AlGaAs/GaAs lasers. Summarizing the results of aging test performed so far and those, which are in progress, we may conclude that they are in agreement with the similar studies for the state-of-the-art, InGaAs/GaAs lasers.

5. Thermal properties of lasers

The temperature at the facet has a critical role in device reliability and performance. Catastrophic optical damage (COD) failure of a laser device occurs at the facet and is caused by absorption of light at the facet which leads to a local band-gap reduction with consequent increased absorption and temperature rise. The runaway effect leads to device failure. Thus the local facet temperature is indicative of these processes. In addition the lateral temperature profile creates a refractive index profile which has a strong effect on device performance. The lateral refractive index profile induced by a non-uniform junction heating plays a dominant role in determining lateral modes and emission characteristics of broad-area lasers during continuous (CW) and long-pulse operation. This is due to thermal focusing caused by temperature induced lateral index profile. Understanding and characterizing these thermal effects is important to development of high power CW lasers. We have developed an in-situ measurement technique for spatially resolved facet temperature

measurements. The method allows for facet temperature mapping under differing operating conditions and assessment of degradation of facets caused by high densities of optical field in the resonator. The measurements also qualify the bonding quality and optimum choice of submount material for heat removal.

5.1. Temperature mapping system. Figure 6 shows the experimental set-up developed for the thermoreflectance measurements of facet heating in semiconductor lasers. The temperature induced changes of the probe beam reflectivity are generally small ($\sim 10^{-5}K^{-1}$) and dependent on the probe beam wavelength. We limit ourselves to single wavelength measurements and perform mapping of the temperature distribution, using calibration described in the subsequent section.

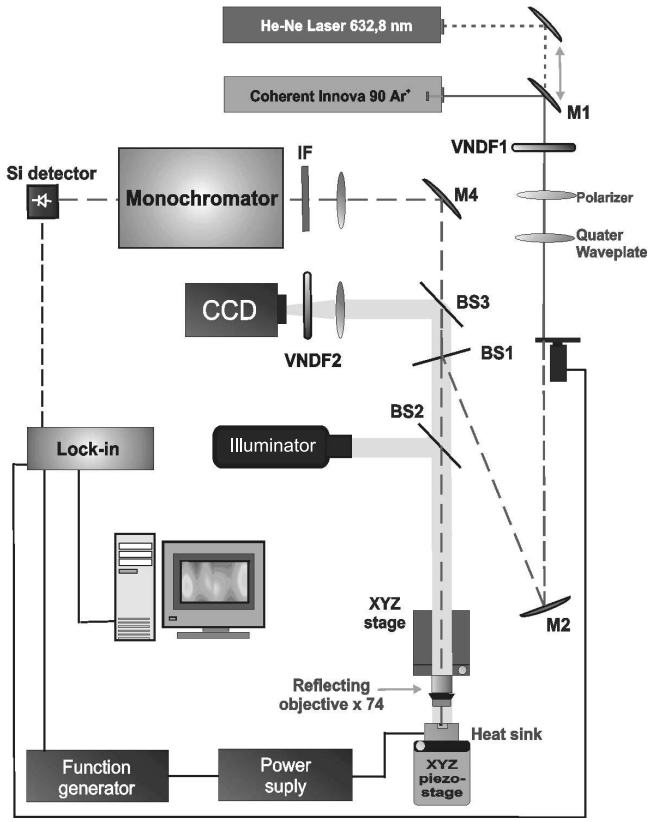

Fig. 6. The experimental set-up for thermoreflectance measurements of facet heating in semiconductor lasers

The dimensions that are of interest are the active region (typically 1 μm high by 50–200 μm wide) and the surrounding regions through which the heat is dissipated. This will amount to several 10 s of microns in the height direction. The spatial resolution of the system is determined by: (1) probe beam focusing and (2) positioning accuracy of translation stages. The probe beam can be focused, using special techniques, down to single micron diameter. The piezoelectric transducers allow 300×300 μm^2 scanning range with 0.2 μm positioning accuracy. The vertical positioning is also done by piezoelectric transducer. The positioning of the laser facet in the focal plane of the optical system is crucial for focusing. The probing beam focusing on the sample is done with reflecting microscope objective. Because of its all reflecting construction it is free from chromatic aberration. The objective consists of a small convex primary mirror and a larger concave secondary mirror. The experiments showed that reflecting objective has clear advantages over refracting objectives of equivalent aperture and focal length. The software for the controlling x-y-z microstages movement and data acquisition uses Lab View platform. The movement of the piezoelectric stages is controlled by IEEE interface.

The thermoreflectance mapping system has been tested for various modes of operation. It can be used for simple reflectance (R) measurements, relative (differential) reflectance measurements ($\Delta R/R$ for given wavelength λ and spectral thermoreflectance measurements. The relative variation of reflectance ($\Delta R/R$ is linear versus the temperature variation ΔT:

$$\Delta R/R = k\Delta T, \quad (1/k = C_{TR}) \tag{10}$$

with C_{TR} being thermoreflectance coefficient. An accurate calibration method is an essential element of any quantitative thermometry techniques. This is of particular importance for the thermoreflectance studies of semiconductor lasers, whose constituent materials have optical properties that are not well-characterized or can vary depending on the processing details. Very few data exist for the absolute values of C_{TR} (thermoreflectance coefficient) in the literature. Reported values on facet temperature scatter in the wide range under high power operation, although each measurement technique is based on the temperature dependence of inherent material parameters, such as refractive index and energy gap. Therefore, the absolute facet temperatures reported are difficult to compare. Due to the fact that the coefficient C_{TR} depends both on probed material, and the experimental conditions, it should not be taken from the literature, but rather determined in-situ, on the probed sample itself. The value of the thermoreflectance constant for the probe beam wavelength ($\lambda = 632.8$ nm, used in this work equals 8×10^3 K.

The example of temperature distribution maps for different supply currents, for the laser mounted p-side down on SiC submount and subsequently on the copper heat sink is shown in Fig. 7. The temperature increase is negligible, even at very high emitted powers, under CW operation. This is because of the quality of the structure and very efficient heat removal. However, for not optimized devices the temperature increase on the mirror can easily exceed 100 K, which may eventually result in serious damage of the mirror and the whole laser.

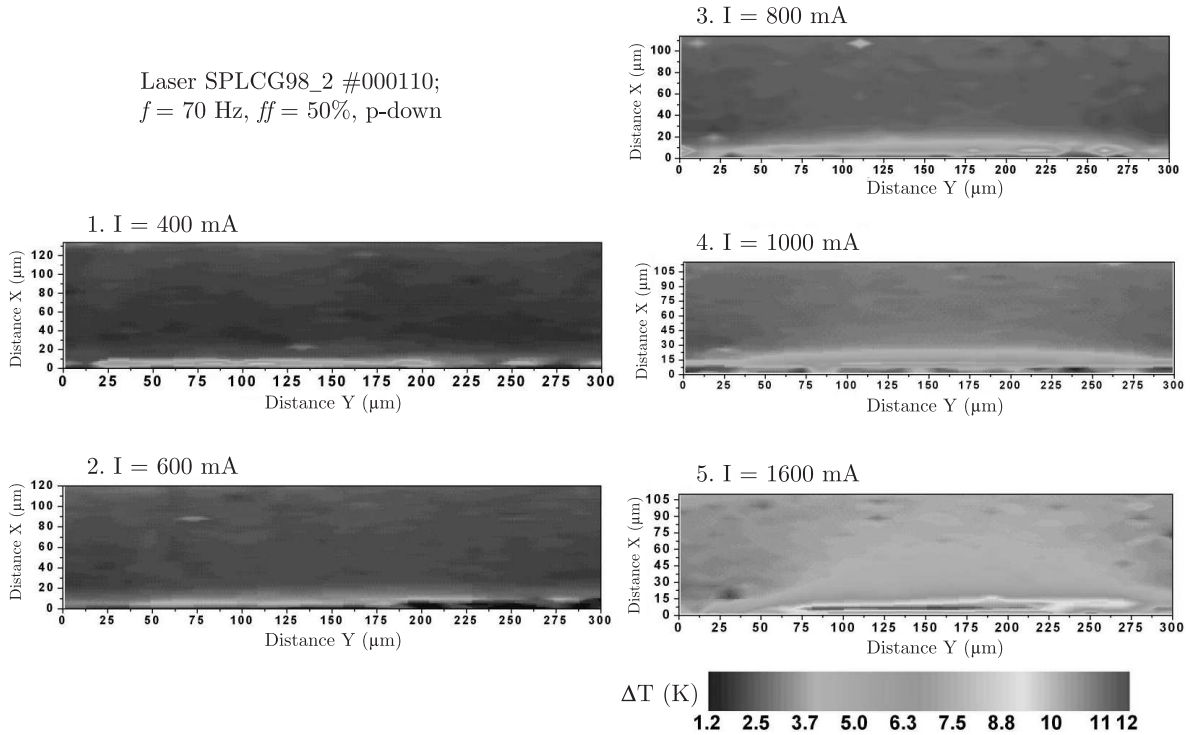

Fig. 7. The temperature distribution maps for different supply currents, for the laser mounted p-side down

6. Conclusions

We have developed MBE technology of strained layer CW InGaAs/GaAs SCH SQW lasers operating at 980-nm band. Broad contact, pump lasers were fabricated in stripe geometry using Schottky isolation and ridge waveguide construction. Threshold current densities of the order of $J_{th} \approx 280$ A/cm^2 and differential quantum efficiency $\eta = 0.40$ W/A (41%) from one mirror were obtained. The wall-plug efficiency of the uncoated lasers was 38%. The record wall-plug efficiency for AR/HR coated devices was equal to 54%. Theoretical estimation of above mentioned quantities were $J_{th} = 280$ A/cm^2 and $\eta = 0.47$ W/A respectively. Degradation studies revealed that uncoated devices did not show any appreciable degradation after 1000 hrs of CW operation with 50 mW of emitted power. Similar life tests, with positive results, are ongoing for AR/HR coated devices already for 1500 hrs at the time of writing this paper. These results are acceptable even considering such demanding applications as pump source for EDFAs. There is however a need for more systematic measurements in CW condition for both, structures with and without coatings, as it is necessary to have better statistics of fabricated lasers reliability. We have also developed new technique to monitor the laser facets heating in real time and to correlate these measurements with device performance and reliability. The method is based on thermoreflectance, which is a modulation technique relaying on periodic facet temperature modulation induced by pulsed current supply of the laser. The periodic temperature change of the laser induces variation of the refractive index and consequently modulates probe beam reflectivity. The technique has a spatial resolution of about ~ 1 μ and temperature differences of a degree can be measured. It can be applied to any kind of edge emitting lasers or laser bars.

Acknowledgements. This work has been supported by KBN grant PBZ -MIN-009/T11/2003.

References

[1] P. Derry and A. Yariv, "Ultralow-threshold graded-index separate-confinement singlequantum well burried heterostructure (Al,Ga)As lasers with high reflectivity coatings", *Appl. Phys. Lett.* 50, 1773 (1987).

[2] W.T. Tsang, "Extremely low threshold (Al,Ga)As modified multiquantum well heterostructure lasers grown by molecular beam epitaxy", *Appl. Phys. Lett.* 39, 786 (1981).

[3] K. Prosyk, J.G. Simmons and J.D. Evans, "Well number, length, and temperature dependence of efficiency and loss in InGaAsP-InP compressively strained MQW ridge wavequide lasers at 1.3 μm", *IEEE J. Quantum Electron.* QE-33, 1360 (1997).

[4] K. Prosyk, J.G. Simmons and J.D. Evans, "A systematic empirical study of the well number and length on the temperature sensitivity of the threshold current in InGaAsP-InP MQW lasers", *IEEE J. Quantum Electron.* QE-34, 535 (1998).

[5] P.W.A. Mc Ilroy, A. Kurobe and Y. Uematsu, "Analysis and application of theoretical gain curves to the design of multi-quantum well lasers", *IEEE J. Quantum Electron.* QE-21, 1958 (1985).

[6] A. Kurobe, H. Furuyama, S. Naritsuka, N. Sugiyama, Y. Kokubun and M. Nakamura, "Effects of well number, cavity length, and facet reflectivity on the reduction of threshold current of GaAs/AlGaAs multiquantum well lasers", *IEEE J. Quantum Electron.* QE-24, 635 (1988).

[7] J.Z. Wilcox, G.L. Peterson, S. Ou, J.J. Yang, M. Jansen and D. Schechter, "Gain- and threshold-current dependence for multiple-quantum well lasers", *J. Appl. Phys.* 64, 6564 (1988).

[8] S.P. Cheng, F. Brillouet and P. Correc, "Design of quantum well AlGaAs-GaAs stripe lasers for minimization of threshold current-Application to ridge structures", *IEEE J. Quantum Electron.* QE-24, 2433 (1988).

[9] M. Rosenzweig, M. Mohrle, H. Duser and H. Venghaus, "Threshold-current analysis of InGaAs-InGaAsP multiquantum well separate-confinement lasers", *IEEE J. Quantum Electron.* QE-27, 1804 (1991).

[10] H.C. Casey and Jr., M.B. Panish, *Heterostructure Lasers*, Academic Press, New York, 1978.

[11] T. Strite and G. Hoven, "Trends in pump laser diode markets and technology", *Lightwave* 16 (2), 55–62 (1999).

[12] J.J. Coleman, "Strained-layer quantum well heterostructure lasers", *Thin Solid Films* 216, 68–71 (1992).

[13] S.D. Offsey, W.J. Schaff, L.F. Lester, L.F. Eastman and S.K. McKernan, "Strained-layer InGaAs-GaAs-AlGaAs lasers grown by molecular beam epitaxy for high speed modulation", *IEEE J. Quantum Electronics* QE-27, 1455–1462 (1991).

[14] M. Bugajski, M. Kaniewska, K. Regiński, A. Maląg, S. Łepkowski and J. Muszalski, "GRIN SCH SQW AlGaAs/GaAs lasers grown by molecular beam epitaxy: Modeling and operating characteristics", *Proc. SPIE* 3186, 310 (1997).

[15] M. Bugajski, M. Kaniewska, K. Regiński, J. Muszalski, D. Kryńska and A. Litkowiec, "GRIN SCH SQW AlGaAs/GaAs lasers grown by molecular beam epitaxy", *Electron Technology* 29, 346–350 (1996).

[16] *PICS 3D Instruction Manual*, Crosslight Software Inc., CA 1998

[17] S.L. Chuang, "Efficient band-structure calculation of strained quantum-wells", *Phys. Rev.* B43, 9649–9661 (1991).

[18] W.W. Chow, S.W. Koch and M. Sargent III, *Semiconductor Laser Physics*, Springer-Verlag, Berlin Heidelberg, 1994.

[19] K. Regiński and M. Bugajski, "MBE technology of semiconductor quantum well lasers", *Opto-Electron. Rev.* 4, 101–116 (1996).

[20] J. Kątcki, J. Ratajczak, J. Adamczewska, F. Phillip, N.Y. Jin-Phillip, K. Regiński, and M. Bugajski, "Formation of dislocations in InGaAs/GaAs heterostructures", *Physica Status Solidi (a)* 171, 275–282 (1999).

[21] J. Kątcki, J. Ratajczak, F. Phillip, N.Y. Jin-Phillip, M. Shiojiri, K. Regiński and M. Bugajski, "TEM study of the formation of defects in AlGaAs/GaAs and InGaAs/GaAs heterostructures", *Electron Technology* 32, 343–347 (1999),

[22] S.L. Chuang, *Physics of Optoelectronic Devices*, Wiley Interscience Publication, New York, 1995.

[23] M. Bugajski and M. Godlewski, "Optical probing of interface disorder in semiconductor nanostructures", *Electron Technology* 31, 159–161 (1998).

[24] M. Bugajski, B. Mroziewicz, K. Regiński, M. Zbroszczyk and A. Maląg, "Optical laser pumps InGaAs/GaAs to the optical waveguide amplifiers EDFA type", *Proc. of the VI Symp. Laser Technique*, Szczecin-Świnoujście 1, 137–141 (1999), (in Polish).

[25] M. Bugajski, K. Regiński, B. Mroziewicz, J.M. Kubica, P. Sajewicz, T. Piwoński, and M. Zbroszczyk, "High-performance 980-nmstrained-layer InGaAs/GaAs quantum-well lasers", *Optica Applicata* 31, 267–271 (2001).

[26] T. Piwoński, P. Sajewicz, J.M. Kubica, M. Zbroszczyk, K. Regiński, B. Mroziewicz and M. Bugajski, "Long-wavelength strained-layer InGaAs/GaAs quantum-well lasers grown by molecular beam epitaxy", *Microwave and Optical Technology Letters* 29, 75–77 (2001).

[27] A. Larsson, J. Cody and R.J. Lang, "Strained-layer InGaAs/GaAs/AlGaAs single quantum well lasers with high internal quantum efficiency", *Appl. Phys. Lett.* 55, 2268–2270 (1989).

[28] A. Larsson, S. Forouhar, J. Cody, R.J. Lang and P.A. Anderson, "A 980 nm pseudomorfic single quantum well laser for pumping erbium-doped optical fiber amplifiers", *IEEE Photonic Technology Letters* PTL-2, 540–542 (1990).

[29] C. Shieh, J. Mantz, H. Lee, D. Ackley and R. Engelman, "Anomalous dependence of threshold current on stripe width in gain-guided strained-layer InGaAs/GaAs quantum well lasers", *Appl. Phys. Lett.* 54, 2521–2523 (1989).

[30] K.J. Beernink, P.K. York, J.J. Coleman, "Dependence of threshold current density on quantum well composition for strained-layer InGaAs-GaAs lasers by metalorganic chemical vapor deposition", *Appl. Phys. Lett.* 55, 2585–2587 (1989).

[31] K.J. Beernink, P.K. York, J.J. Coleman, R.G. Waters, J. Kim and C.M. Wayman, "Characterization of strained-layer InGaAs-GaAs lasers with quantum wells near the critical thickness", *Appl. Phys. Lett.* 55, 2167–2169 (1989).

[32] H. Horie, H. Ohta and T. Fujimori, "Reliability improvement of 980-nm laser diodes with a new facet passivation process", *IEEE J. Selected Topics in Quantum Electronics* 5, 832–838 (1999).

[33] M. Okayasu, M. Fukuda, T. Takeshita and S. Uehara, "Stable operation (over 5000 h) of high power 0.98 μm InGaAs-GaAs strained quantum well ridge waveguide lasers for pumping Er^{3+}-doped fiber amplifiers", *IEEE Photonic Technology Letters* PTL-2, 689–691 (1990).

[34] M. Fukuda, M. Okayasu, J. Temmyo and J. Nakano, "Degradation behavior of 0.98-μm strained quantum well InGaAs/AlGaAs lasers under high-power operation", *IEEE J. Quantum Electronics*, QE-30, 471–476 (1994).

[35] S.E. Fischer, R.G. Waters, D. Fekete, J.M. Ballantyne, Y.C. Chen and B.A. Soltz, "Long-lived InGaAs quantum well lasers", *Appl. Phys. Lett.* 54, 1861–1863 (1989).